Solution-processed Perovskite Optoelectronics

Lih Y. Lin
Electrical Engineering Department
University of Washington
Seattle, WA, USA
lylin@uw.edu

Chen Zou
Electrical Engineering Department
University of Washington
Seattle, WA, USA
chenzou@uw.edu

***Abstract*—We discuss our recent work on perovskite laser, LED, and phototransistor using solution-processed $CsPbX_3$ quantum dots.**

Keywords—perovskite, quantum dots, laser, LED, phototransistor

I. Introduction

Solution-processed nanomaterials offer a promising route to overcome the grand challenge of integrated light sources on Si and flexible substrates due to their wide fabrication compatibility, but they have not achieved satisfactory performance in both efficiency and stability. In recent years, metal halide perovskites have emerged as a highly promising newcomer among photonic materials. They exhibit high charge mobility [1], sharp optical absorption edges and high absorption coefficients comparable to GaAs [2], as well as an unusual defect tolerance [3]. The materials were first applied to photovoltaics and resulted in record certified research solar cell power conversion efficiencies >22% in less than four years [4]. The outstanding performance suggests their promise for light-emitting and other photodetection applications, and many research efforts have been made in this field. Here, we present and discuss our work on perovskite quantum dot (QD) vertical cavity lasers with low threshold (0.39 μJ/cm^2), LEDs with high stability, and broad-band hybrid phototransistor with high sensitivity.

II. Low-threshold Perovskite QD Vertical Cavity Lasers

All-inorganic cesium lead bromide ($CsPbBr_3$) perovskite quantum dots (QDs) have recently attracted much attention as highly promising solution-processed materials for next-generation light-emitting applications [5-8]. They utilize the advantages of QDs and perovskite materials together, therefore have great potentials in achieving high optical gain with good stability. We have demonstrated an ultra-low lasing threshold (0.39 μJ/cm^2) from a vertical cavity surface emitting laser (VCSEL) structure consisted of a $CsPbBr_3$ QD film and two distributed Bragg reflectors (DBR) [9]. Temperature dependence of the lasing threshold and ambient stability of the device were also characterized. The $CsPbBr_3$ QDs provide better stability and enable device operations over 5h/1.8×10^7 optical pulse excitations under ambient conditions. Stable lasing operation was achieved under both short pulse (femtosecond) and quasi-continuous-wave (nanosecond) operations.

The device structure is shown in Figure 1(a). The $CsPbBr_3$ QD film is sandwiched between two commercially available DBRs. A 400 nm, 50 fs pulse laser was first used as the pump source. The transmission spectrum of the DBR is shown in Figure 1(b). The DBR has high transmittance in 375-500 nm wavelength region, which allows the use of 400 nm as the pump source wavelength. The transmittance of the DBR is close to 0% in the range of 500-600 nm, where the photoluminescence (PL) peak of $CsPbBr_3$ QDs is located, allowing high-Q resonance to occur between two DBRs. Figure 2(a) shows the PL spectra of our VCSEL device under different pump fluence. The inset shows the emission beam captured by a CCD camera. Below lasing threshold, the emission is mainly from spontaneous emission, which is blocked by the DBR mirror, thus there is almost no signal detected by the spectrometer [10]. Above the lasing threshold, a narrow peak located at λ=522 nm starts to appear. As the pump fluence continues to increase, the peak intensity increases dramatically. The full width half maximum (FWHM) of the emission spectra above the lasing threshold is about 0.9 nm, which is much narrower than that of amplified spontaneous emission from $CsPbBr_3$ QD thin film (~8 nm). Figure 2(b) shows the the output intensity versus input pump

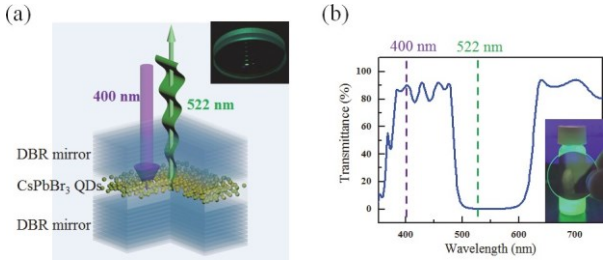

Fig. 1. (a) The schematic diagram of the $CsPbBr_3$ QD VCSEL. Inset: photograph of the VCSEL in operation. (b) Transmission spectrum of the DBR. Inset: photograph of the DBR in front of the green-emission $CsPbBr_3$ QD solution. The DBR reflects the green light while transmitting the UV light.

978-1-5386-1016-9/18/$31.00 ©2018 IEEE

fluence (L-L curve), a L-L kink at 0.39 uJ/cm^2 can be observed, which demonstrates the occurrence of stimulated emission and lasing above the threshold. The time resolved spectrogram was obtained by a streak camera, as shown in Figure 2(c). A narrow emission band around 522 nm appears as an intense ellipse spot in the spectrogram. The corresponding time-resolved emission intensity decay trace is plotted in Figure 2(d). The fast decay (~10 ps) is attributed to a stimulated emission process, which is consistent with other reported values of stimulated emission lifetime for perovskite materials [7, 11].

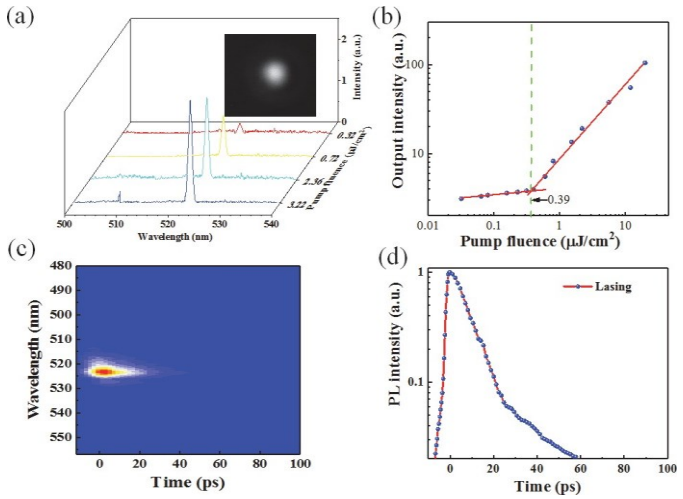

Fig. 2. (a) The emission spectra under different pump fluences from the $CsPbBr_3$ QD VCSEL. Inset: Far-field image of the emission beam from the VCSEL above the lasing threshold. (b) L-L curve for the $CsPbBr_3$ QD VCSEL, with a kink at 0.39 μJ/cm^2. (c) Time-resolved spectrogram and (d) time-dependent emission intensity above the lasing threshold. The device was excited at λ= 400 nm with 50 fs laser pulses.

In order to study the temperature dependent performance of our VCSEL devices. We measured the lasing threshold at temperature range from 120 to 295 K with the femtosecond pulsed laser as the pump source. As shown in Figure 3(a), the lasing threshold decreases steadily when temperature decreases, and finally reaches 0.15 μJ/cm^2 at 120 K. We attribute this to reduced thermal heat during lasing operation and decreased Auger recombination loss at low temperature. The stability of perovskite optoelectronics is still a big concern in perovskite research community. We define an 80%-lifetime (T_{80}) as the time it takes for the emission intensity decreases to 80% of the initial value. As shown in Figure 3(b), the device under 50 fs pump pulses shows higher stability (T_{80} > 5h/1.8 × 10^7 pulses) while the emission intensity decreases much faster under 5 ns pump pulses (T_{80} ~ 2h).

III. Perovskite QD LEDs with Red Emission and High Stability

Although Perovskite materials ($MAPbBr_3$, $FAPbBr_3$ and $CsPbBr_3$) have been utilized to fabricated green LEDs with a highest L_{70} lifetime (EL intensity decreases to 70% of initial value, an IES TM21 standard) of >900 min and a EQE of

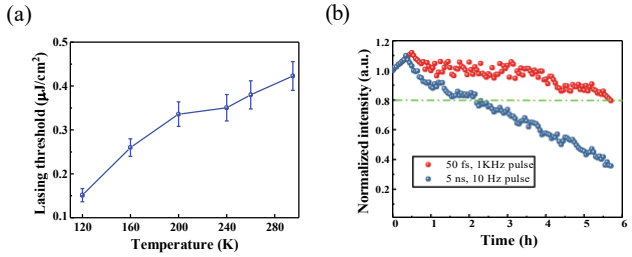

Fig. 3. (a) Lasing threshold dependence on temperature for the $CsPbBr_3$ QD VCSEL. (b) Stability characterizations of the device under fs (red) and ns (blue) pulsed excitation with pump fluences set at 1.1 P_{th}. The measurements were performed at room temperature under ambient conditions.

0.15% reported [12], there has been little published work on the stability of perovskite LEDs with red emission, likely due to the small Goldschmidt tolerance factor of $CsPbI_3$ or $MAPbI_3$, which is an indicator for the stability of crystal structures as determined by the relative size of the constitutional ions. $MAPbI_3$ can be cubic phase at room temperature; however, it degrades fast and transforms to orthorhombic phase in ambient condition. A perovskite LED based on $MAPbI_{3-x}Cl_x$ thin film with emission wavelength centered at 770 nm was reported to achieve 0.48% maximum EQE and only 2 min L_{70} lifetime [13]. $CsPbI_3$ is usually not cubic phase at room temperature, heating above 300 ºC is the prerequisite for $CsPbI_3$ to obtain the cubic phase, which gives LEDs and solar cells based on $CsPbI_3$ better efficiency and performance [14]. Recently, it was reported [15] that by utilizing an improved purification approach, nanocrystal surfaces can be used to stabilize cubic phase $CsPbI_3$ at room temperature, far below the phase transition temperature for thin film or bulk materials. This finding indicates $CsPbI_3$ QDs a great candidate for stable red-emission perovskite LEDs. Utilizing the above-mentioned improved purification method, we have achieved a highly stable $CsPbI_3$ QD LED with red emission [16]. The device achieved an external quantum efficiency (EQE) of 0.21% at 6 V and great operational stability in ambient condition, with a L_{70} lifetime of 16 h and 1.5 h under a constant driving bias of 5V and 6V (maximum EQE operation) respectively. Furthermore, the device can work under a higher voltage of 7V (maximum luminance operation) and maintain 50% of its initial EL intensity after 500 s. These findings suggest the potential application of $CsPbI_3$ QDs for stable red LEDs.

The LED structure and cross-sectional SEM image are shown in Figure 4(a) and (b). The ITO electrode is used as anode, PEDOT:PSS and TPBI function as hole transport layer (HTL) and electron transport layer (ETL) respectively. The $CsPbI_3$ QD thin film is sandwiched between HTL and ETL as the active layer, where electron and holes combine to emit photons. LiF (1nm)/Al (100nm) is used as cathode. Figure 4(c) shows the energy level diagram of the LED structure, which also exhibits the hole and electron transport path. The luminance-current density-voltage (L-J-V) characteristics of the device are shown in Figure 5(a). The $CsPbI_3$ QD LED shows clear diode characteristics with a low turn-on voltage V_{on} of 3V. The LED achieves a maximum luminance of 7.2

cd/m^2 at 7V. The current efficiency and EQE dependence on the applied voltage are shown in Figure 5(b). A maximum current efficiency of 0.012 cd/A and EQE of 0.21% are achieved at an applied voltage of 6V. The EQE can be further increased by enhancing the PLQY and the conductivity of $CsPbI_3$ QD thin films besides a better device design to minimize the energy barrier at PEDOT:PSS/$CsPbI_3$ QDs interface. Figure 5(c) shows the Electroluminescence (EL) spectra of the $CsPbI_3$ QD LED at different voltages. The EL spectra are centered at 693 nm with a FWHM of 32 nm. The CIE coordinate of the LED emission is (0.70,0.26), on the red corner of the CIE color diagram as shown in Figure 5(d).

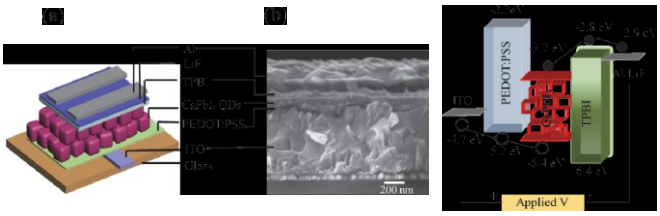

Fig. 4. (a) The schematic device structure. (b) The cross-sectional SEM image of the LED. (c) The energy level diagram of the device.

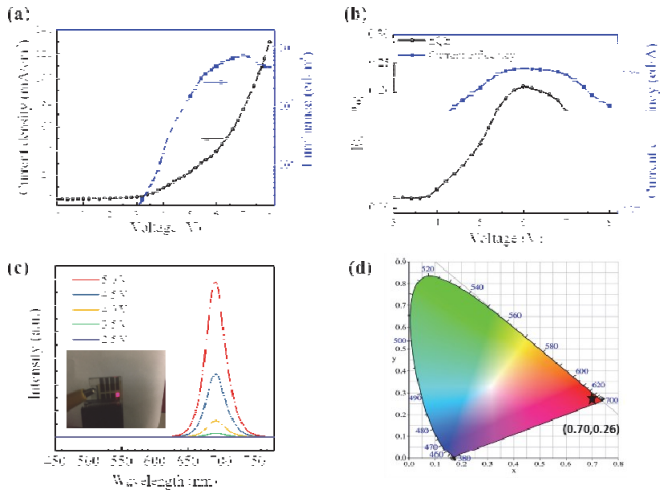

Fig. 5. (a) Current density and luminance as a function of voltage, and (b) external quantum efficiency and current efficiency versus voltage. (c) EL spectra at different applied voltages. Inset: Photograph of the device in operation. (d) CIE coordinates of the emission color from the $CsPbI_3$ QD LED.

We further characterized the operation stability of our $CsPbI_3$ QD LED under different applied voltages. As shown in Figure 6(a), The L_{70} lifetime of the LED at a constant voltage of 5V is about 16 hours, the initial luminance is 1.5 cd/m^2, which is the close to minimum luminance (1 cd/m^2) our eyes can catch sight of. Working at the bias of 6V, the LED shows the maximum EQE and has a L_{70} lifetime of 1.5 hours, the thermal heat and increased Auger loss due to higher injection current may contribute to a shorter lifetime. When the device starts to work under the condition of maximum luminance at 7V, an immediate luminance degradation occurred, and the device can only survive for several minutes.

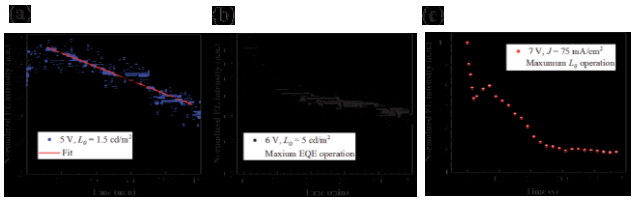

Fig. 6. Operational stability of the $CsPbI_3$ LED working at (a) 5 V, (b) 6 V where maximum EQE is reached, and (c) high injected current density condition (7 V, J = 75 mA/cm^2), where maximum luminance is achieved. The measurements were conducted at room temperature in ambient environment.

IV. Perovskite QD Heterojunction Phototransistors

As mentioned above, all-inorganic perovskite QDs ($CsPbX_3$, X= Cl, Br or I) have been widely used in perovskite optoelectronics including solar cells, LEDs and lasers. Recently, several works have also initialized applications of perovskite QDs in photodetectors [17, 18]. However, the responsivity is restricted by poor charge transport between QDs. A practical way to improve the responsivity is to adopt the layered heterojunction (LHJ) structure. With the help of LHJ, the light-generated electrons and holes are separated into different paths, facilitating the carrier extraction. We demonstrated a phototransistor based on the LHJ structure consisted of $CsPbI_3$ QDs and a conjugated polymer (DPP-DTT [19]). The device exhibits great optoelectronic properties with a responsivity up to 110 A/W, a specific detectivity (D^*) of 2.9×10^{13} Jones and a light-dark current ratio of 6×10^3.

Furthermore, applying the narrow-bandgap DPP-DTT as a complementary light absorber, a wide photodetection range from 350-1000 nm was realized, demonstrating promising applications of the perovskite heterojunction phototransistor in near-infrared (NIR) detection.

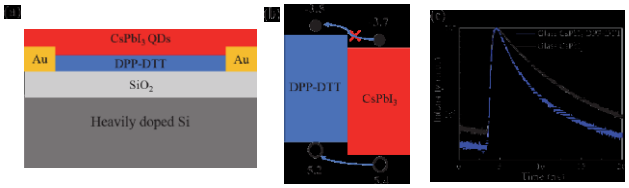

Fig. 7. (a) The schematic structure of the heterojunction phototransistor. (b) Energy level diagram of the hybrid film (unit: eV). (c) Transient PL decay curves of the hybrid film and pristine $CsPbI_3$ QD film.

The structure of the heterojunction phototransistor is shown in Figure 7(a). A heavily doped silicon wafer with 200 nm thick SiO_2 was used as the substrate. The heavily doped silicon is connected as the bottom gate electrode. Gold electrodes are thermally evaporated to form drain-source channels with a length and width of 100 um and 1 mm respectively. Figure 7(b) shows the energy level diagram of the heterojunction structure. Due to the energy barrier for electrons at the $CsPbI_3$ QDs/DPP-DTT interface, electrons tend to accumulate in the perovskite layer, whereas holes transfer to the DPP-DTT layer and recirculate many times in drain-source channels due to high hole mobility (~ 0.2 cm^2 V^{-1} s^{-1}) and long carrier lifetime of DPP-DTT. The time-resolved PL decay tests of the hybrid film and pristine $CsPbI_3$ QD film were performed. As shown in

Figure 7(c), the shorter PL lifetime of the hybrid film compared to that of pristine $CsPbI_3$ QD film indicates the efficient charge transfer near the interface.

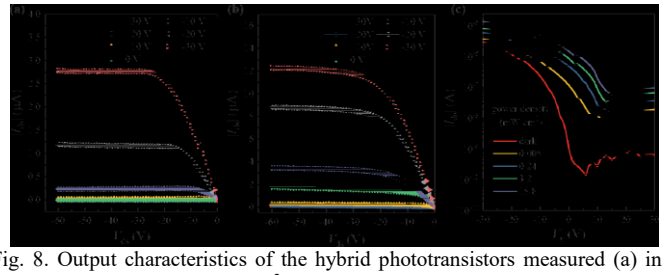

Fig. 8. Output characteristics of the hybrid phototransistors measured (a) in dark and (b) under 18.8 mW/cm^2 light irradiation. (c) Transfer characteristics in dark and under different light intensities.

The output characteristics (I_{ds} vs V_{ds}) of the heterojunction phototransistor were measured in dark condition and under the light irradiation of 18.8 mW/cm^2 respectively, as shown in Figure 8(a) and (b). They all show typical p-type linear to saturation transistor characteristics. Upon 405 nm light illumination, the drain-source current increases noticeably compared to that measured in dark condition at the same gate voltage. The transfer characteristics ((I_{ds} vs V_{gs}) of the heterojunction phototransistor measured in dark and under different light intensities (P = 0.008, 0.24, 3.2, 18.8 mW/cm^2) are shown in Figure 8(c). In dark condition, I_{ds} is at the level of 1 nA when the applied gate voltage is positive. However, I_{ds} dramatically increase when the gate voltage moves along the negative direction due to the field effect. With increasing light intensity, the transfer characteristic curve maintains similar shape but the threshold moves to the positive direction due to photogating effect [20].

V. Conclusions

Solution-processed perovskite materials have shown high promise for optoelectronic devices. All-inorganic $CsPbX_3$ perovskite QDs have the unique advantages of high PL quantum yield and stability. Upon further improvement in material reliability and device structures, perovskite materials have strong potentials in creating high impacts in optoelectronics.

Acknowledgment

We thank Dr. Chun-Ying Huang and Dr. Erin Sanehira of the University Washington, Dr. Joseph Luther of National Renewable Energy Laboratory, for discussions and contributions to the work. Chen Zou thanks UW Clean Energy Institute for financial support through graduate fellowship.

References

[1] C. S. Ponseca, T. J. Savenije, M. Abdellah, K. Zheng, A. Yartsev, T. Pascher, T. Harlang, P. Chabera, T. Pullerits, A. Stepanov, J.-P. Wolf, and V. Sundström, "Organometal Halide Perovskite Solar Cell Materials Rationalized: Ultrafast Charge Generation, High and Microsecond-Long Balanced Mobilities, and Slow Recombination," *Journal of the American Chemical Society,* vol. 136, pp. 5189-5192, 2014.

[2] S. De Wolf, J. Holovsky, S.-J. Moon, P. Löper, B. Niesen, M. Ledinsky, F.-J. Haug, J.-H. Yum, and C. Ballif, "Organometallic Halide Perovskites: Sharp Optical Absorption Edge and Its Relation to Photovoltaic Performance," *The Journal of Physical Chemistry Letters,* vol. 5, pp. 1035-1039, 2014.

[3] W.-J. Yin, T. Shi, and Y. Yan, "Unusual defect physics in $CH_3NH_3PbI_3$ perovskite solar cell absorber," *Applied Physics Letters,* vol. 104, p. 063903, 2014.

[4] *National Renewable Energy Laboratory, Best Research-Cell Efficiencies Chart*. Available: https://www.nrel.gov/pv/assets/images/efficiency-chart.png

[5] J. Song, J. Li, X. Li, L. Xu, Y. Dong, and H. Zeng, "Quantum Dot Light-Emitting Diodes Based on Inorganic Perovskite Cesium Lead Halides ($CsPbX_3$)," *Adv Mater,* vol. 27, pp. 7162-7, 2015.

[6] W. Deng, X. Xu, X. Zhang, Y. Zhang, X. Jin, L. Wang, S. T. Lee, and J. Jie, "Organometal Halide Perovskite Quantum Dot Light‐Emitting Diodes," *Advanced Functional Materials,* vol. 26, pp. 4797-4802, 2016.

[7] Y. Wang, X. Li, J. Song, L. Xiao, H. Zeng, and H. Sun, "All-Inorganic Colloidal Perovskite Quantum Dots: A New Class of Lasing Materials with Favorable Characteristics," *Adv Mater,* vol. 27, pp. 7101-8, 2015.

[8] S. Yakunin, L. Protesescu, F. Krieg, M. I. Bodnarchuk, G. Nedelcu, M. Humer, G. De Luca, M. Fiebig, W. Heiss, and M. V. Kovalenko, "Low-threshold amplified spontaneous emission and lasing from colloidal nanocrystals of caesium lead halide perovskites," *Nature Communications,* vol. 6, p. 8056, 2015.

[9] C. Y. Huang, C. Zou, C. Y. Mao, K. L. Corp, Y. C. Yao, Y. J. Lee, C. W. Schlenker, A. K. Y. Jen, and L. Y. Lin, "$CsPbBr_3$ Perovskite Quantum Dot Vertical Cavity Lasers with Low Threshold and High Stability," *Acs Photonics,* vol. 4, pp. 2281-2289, 2017.

[10] S. Chen, C. Zhang, J. Lee, J. Han, and A. Nurmikko, "High‐Q, Low‐Threshold Monolithic Perovskite Thin‐Film Vertical‐Cavity Lasers," *Advanced Materials,* p. 1604781, 2017.

[11] S. W. Eaton, M. Lai, N. A. Gibson, A. B. Wong, L. Dou, J. Ma, L.-W. Wang, S. R. Leone, and P. Yang, "Lasing in Robust Cesium Lead Halide Perovskite Nanowires," *Proceedings of the National Academy of Sciences,* vol. 113, pp. 1993-1998, 2016.

[12] Z. Wei, A. Perumal, R. Su, S. Sushant, J. Xing, Q. Zhang, S. T. Tan, H. V. Demir, and Q. Xiong, "Solution-processed highly bright and durable cesium lead halide perovskite light-emitting diodes," *Nanoscale,* vol. 8, pp. 18021-18026, 2016.

[13] O. A. Jaramillo-Quintero, R. S. Sanchez, M. Rincon, and I. Mora-Sero, "Bright visible-infrared light emitting diodes based on hybrid halide perovskite with Spiro-OMeTAD as a hole-injecting layer," *The journal of physical chemistry letters,* vol. 6, pp. 1883-1890, 2015.

[14] J. Lin, M. L. Lai, L. T. Dou, C. S. Kley, H. Chen, F. Peng, J. L. Sun, D. L. Lu, S. A. Hawks, C. L. Xie, F. Cui, A. P. Alivisatos, D. T. Limmer, and P. D. Yang, "Thermochromic halide perovskite solar cells," *Nature Materials,* vol. 17, pp. 261-+, 2018.

[15] A. Swarnkar, A. R. Marshall, E. M. Sanehira, B. D. Chernomordik, D. T. Moore, J. A. Christians, T. Chakrabarti, and J. M. Luther, "Quantum dot–induced phase stabilization of α-$CsPbI_3$ perovskite for high-efficiency photovoltaics," *Science,* vol. 354, pp. 92-95, 2016.

[16] C. Zou, C.-Y. Huang, E. Sanehira, M. , J. Luther, and L. Y. Lin, "Highly stable cesium lead iodide perovskite quantum dot light-emitting diodes," *Nanotechnology,* vol. 28, p. 455201, 2017.

[17] K. M. Sim, A. Swarnkar, A. Nag, and D. S. Chung, "Phase Stabilized - CsPbI3 Perovskite Nanocrystals for Photodiode Applications," *Laser & Photonics Reviews,* vol. 12, 2018.

[18] P. Ramasamy, D. H. Lim, B. Kim, S. H. Lee, M. S. Lee, and J. S. Lee, "All-inorganic cesium lead halide perovskite nanocrystals for photodetector applications," *ChemCommun,* vol. 52, pp. 2067-70, 2016.

[19] C. Zou, Y. Xi, C. Y. Huang, E. G. Keeler, T. Feng, S. Zhu, L. D. Pozzo, and L. Y. Lin, "A Highly Sensitive UV–vis‐NIR All‐Inorganic Perovskite Quantum Dot Phototransistor Based on a Layered Heterojunction," *Advanced Optical Materials,* p. 1800324, 2018.

[20] C. Xie, P. You, Z. K. Liu, L. Li, and F. Yan, "Ultrasensitive broadband phototransistors based on perovskite/organic-semiconductor vertical heterojunctions," *Light-Science & Applications,* vol. 6, p. e17023, 2017.